




Renoval: A Novel Annular Fresnel Solar Furnace for Aluminium Melting and Recycling

Pablo Castillo¹  <https://orcid.org/0009-0009-7883-2097>, Cristopher Rozas¹, Francisco Fuentes¹ 
<https://orcid.org/0009-0002-5725-4776>, and Iván Muñoz¹  <https://orcid.org/0000-0001-5895-5924>

¹ Fraunhofer Chile Research, Center for Solar Energy Technologies (CSET), Chile

*Correspondence: Pablo Castillo, pablo.castillo@fraunhofer.cl

Abstract. We present Renoval, a compact Annular Fresnel solar furnace designed and locally manufactured for aluminium remelting and recycling. The 5.3 m², 1200-suns prototype couples a segmented acrylic-mirror reflector to a crucible-in-cavity receiver and two-axis tracking. We report 21 outdoor trials in Santiago, Chile (Nov–May 2025), establishing a repeatable pour/recharge workflow and achieving a maximum daily melt of 1.71 kg under median DNI = 902 W m⁻². To interpret performance and guide scale-up, we develop a six-node lumped thermal model that reproduces pre-pour ramps and melt onset with RMSE = 31.2 °C using measured DNI and logged handling events. An energy-ledger analysis attributes ≈74% of incident solar energy to environmental losses, dominated by the front window (≈40%) and side walls (≈30%), while the productive crucible→aluminium path accounts for only ≈3% over the analyzed window; the remainder is stored in refractory mass. Renoval demonstrates that high-flux, metered remelting with industrial handling can be achieved using locally fabricated hardware, providing a practical pathway for low-emission aluminium recycling in Chile.

Keywords: Concentrated Solar Thermal; Aluminium Remelting; Annular Fresnel; Recycling; Solar Metallurgy

1. Introduction

Industrial heat consumption is projected to increase by 17% by 2030 – an addition of approximately 20 EJ - with countries like China and India accounting for over half of this growth. Despite this, solar thermal energy contributions remain minimal, representing less than 1% of the industry's growth in renewable heat consumption. Nonetheless, solar heat for industrial processes is expected to expand in sectors such as food and beverage, textile and mining [1].

The aluminium industry is a cornerstone of many technologies critical to the energy transition; however, it is also a significant source of CO₂ emission, with nearly 270 Mt of direct emission in 2022 - representing about 3% of global direct industrial CO₂ emissions. While the energy efficiency in aluminium production has improved, there is an urgent need to accelerate the switch to renewables alternatives like biodiesel, hydrogen or near zero-emission electricity [2].

Concentrated solar thermal technologies presents a promising alternative for the aluminium industry. This potential is evidenced by projects like Glasspoint Ma'aden Solar 1, which plans to integrate a 1500 MWth enclosed parabolic trough collector plant into the alumina refinery operations of the Ma'aden Group in Saudi Arabia [3].

High-flux solar furnaces like PROMES-CNRS and PSA SF60 have demonstrated the capability to reach >3000°C for materials processing and thermo-chemical research, validat-

ing the feasibility of high temperature solar heat for metallurgical operations [4], [5]. However, most prior work focuses on generic high-flux experiments rather than repeatable, metered aluminium-scrap remelting with industrial handling and controlled pouring, supported by validated system models; consequently, these facilities have remained experimental test beds rather than precursors to industrial deployment.

In parallel, annular Fresnel concentrators have been proposed and tested as compact, potentially lower-cost alternatives to dishes [6], [7], however, to our knowledge no prototype, end-to-end demonstration for directly heated aluminium remelting for recycling have been reported.

This work presents Renoval, a prototype annular Fresnel solar concentrator-receiver for aluminium remelting and recycling, together with its design, fabrication and outdoor testing. Specifically, we (i) detail the optical and thermal design and manufacturing, (ii) report instrumented outdoor melting trials, (iii) develop and validate a lumped thermal-resistance model against measurements to assess scalability and use-case viability.

2. System Overview

Renoval is a compact, high-flux solar melting system built around a novel annular Fresnel concentrator that delivers concentrated irradiance onto a furnace-like receiver with an internal crucible for aluminium remelting (scraps), as shown in Figure 1. The system integrates sun-tracking and control, thermal/structural components, and the instrumentation for performance monitoring and model validation.

The intended use case of this prototype is the direct solar remelting of aluminium for recycling and casting trials, not primary smelting. The nominal specifications of the prototype are an aperture area 5.3 m^2 , nominal concentration 1200 suns (dimensionless), optical efficiency 0.45, theoretical useful power 2385 W at $\text{DNI} = 1000 \text{ Wm}^{-2}$, rated melt rate 0.3 kg/hour , batch capacity 0.7 kg . The targeted KPIs include absorbed heat, useful heat to melt, thermal efficiency and specific energy consumption.

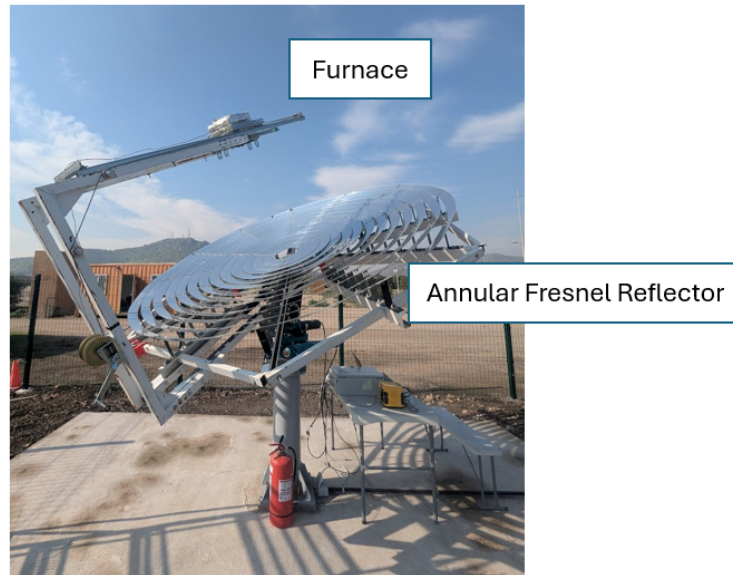


Figure 1. Image of Renoval solar furnace installed on site.

3. Design and manufacturing

The Renoval annular Fresnel concentrator consists of 13 concentric reflective rings spanning an area of 5.3 m^2 (outer radius 1.3 m) and designed with a focal length of 100 cm .

The reflective rings were fabricated from 3 mm-thick acrylic sheets with a silver mirror finish, with a specular reflectance of 0.83. Each ring has a specific tilt angle to reflect incident radiation onto the receiver plane. The rings were divided into 3, 6, and 12 segments depending on their size, avoiding segments longer than 50 cm to minimize deflection under self-weight.

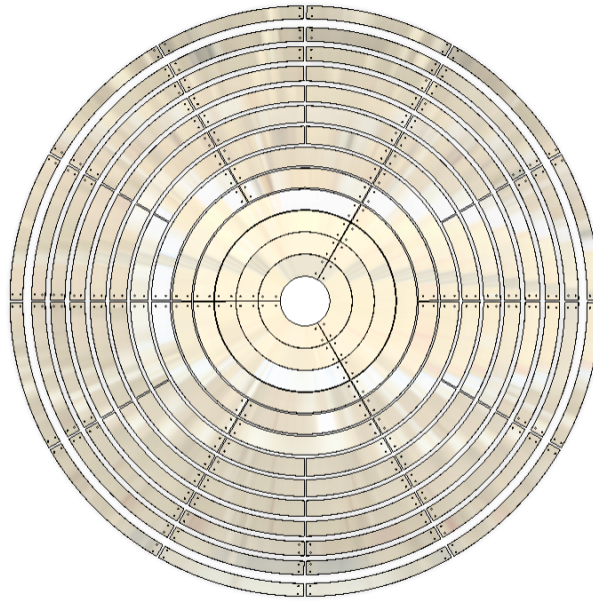


Figure 2. CAD design used for manufacturing the 13 rings used in annular Fresnel reflector.



Figure 3. Image of annular Fresnel reflector installed on site.

The initial receiver consisted of a 20 cm-diameter disk, with which a geometric concentration ratio of approximately 169 suns and an optical efficiency of 0.87 was achieved. However, in later stages the receiver was modified to use a 7.5 cm-diameter graphite crucible, obtaining a geometric concentration ratio of 1200 suns and an optical efficiency of 0.45.

The receiver was built taking a laboratory-grade electric melting furnace as reference, using a high-purity graphite crucible as the aluminium container and insulating firebrick for the furnace body to minimize heat losses to the surroundings. The concentrated solar radiation from the Fresnel reflector enters through the bottom of the furnace, where it is absorbed by the crucible, as shown in Figure 4 and 5. Three crucible models were used, with capacities of 3, 5, and 6 kilograms of gold (the typical crucible sizing standard). The 5-kg model was ultimately selected for the tests.

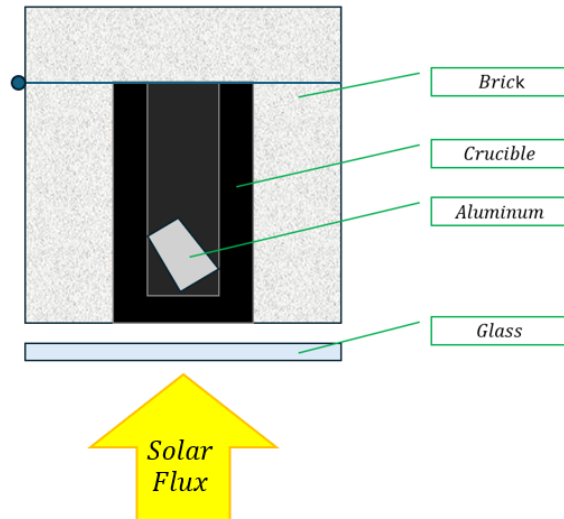


Figure 4. Diagram of the custom-made furnace design for solar aluminum melting.



Figure 5. Images of the two custom-made furnaces manufactured for the Renoval solar furnace

The furnace is mounted at the focal point of the Fresnel array on a rail system for quick handling during casting. This rail system is actuated by a hand-operated winch.

The structure supporting the concentrator was built from stainless-steel sections and later mounted on a ConeDrive dual axis slewing drive system, which allowed positioning of the concentrator about the azimuth and elevation axes. The two-axis motion electronics were

developed by Fraunhofer Chile, enabling automatic sun tracking using a photoresistor-based sensor, as well as manual control of the concentrator via a Bluetooth remote.

4. Solar Melting Experiments

The Renoval concentrator was installed at Parque Caren, Santiago, Chile (33.4351° S, 70.8457° W). Outdoor melting trials were conducted between November and May, 2025, covering summer and autumn conditions. A total of 21 experiments were performed, with typical trial durations of 3 to 5 h. Sky conditions ranged from clear sky to scattered cloudy, with direct normal irradiance (DNI) spanning 850–1080 W·m⁻² and median values around 960 W·m⁻².

Direct normal irradiance was measured using a Kipp & Zonen CHP1 pyrheliometer (accuracy ±1% [8]) mounted on same concentrator structure. Crucible and furnace-wall temperatures were monitored with Omega High Temperature Inconel Overbraided Ceramic Fibre Insulated Type-K thermocouples [9]; one channel recorded at crucible outer wall. Signals were logged at 0.1 Hz (10 s sampling) using Keysight 34972A Data Acquisition Unit. Aluminium charge was weighed before and after trials on a scale (resolution 1 g). The sun-tracking system used a four-quadrant light resistance sensor controller with manual override; emergency manual control was available via a Bluetooth remote controller.

Two aluminium alloys were tested: Alloy 4032 (engine pistons) and alloy 7178 (aeronautical plates). Nominal solidus–liquidus ranges used for operation were 530–570 °C for 4032 alloy and 477–629 °C for 7178 alloy (melting criterion set at liquidus temperature + 10 °C). A trial was initiated if DNI exceeded 800 W·m⁻² under clear-sky conditions.

The operational workflow was refined iteratively to improve stability and melt rates:

1. Pre-load the crucible with ~150 g aluminium (seed pool).
2. Start sun tracking; monitor temperature of crucible–brick continuously.
3. When temperature ≥ (liquidus temperature + 10 °C), charge ~500 g additional aluminium.
4. Resume tracking until temperature ≥ (liquidus temperature + 10 °C) again.
5. Pour ~50% of the liquid aluminium; immediately recharge ~250 g solid feed to maintain a thin liquid pool for enhanced heat transfer.
6. Repeat until the target mass is achieved or crucible can no longer reach the alloy's liquidus temperature.

The computed performance metrics are the following:

1. Melt rate $\dot{m} = \Delta m / \Delta t$ in kg h⁻¹ over each pouring cycle.
2. Absorbed heat $Q_{abs} = \eta_{opt} A_{ap} DNI \Delta t$ with $\eta_{opt} = 0.45$ and aperture $A_{ap} = 5.3 \text{ m}^2$.
3. Useful heat to melt $Q_{use} = m \left[c_p (T_m - T_0) + \Delta h_{fus} \right]$ using $\Delta h_{fus} = 360 \text{ kJ kg}^{-1}$ and $T_0 = 20^\circ\text{C}$.
4. Thermal Efficiency $\eta_{th} = Q_{use} / Q_{abs}$
5. Specific energy consumption $SEC = Q_{abs} / \Delta m$ in kWh kg⁻¹
6. Startup time to first pour: time measured in minutes, from start of tracking to first pour.

Early trials yielded $0.10\text{--}0.20\text{ kg day}^{-1}$ of molten aluminium as procedures were tuned. The maximum daily melt reached 1.71 kg on April 8, 2025, under median $\text{DNI} = 902\text{ W}\cdot\text{m}^{-2}$. A representative time series of crucible temperature and DNI for that day is shown in Figure 6. After a rapid warm-up, the pour/recharge operation keeps the crucible temperature between $520\text{--}600^\circ\text{C}$ while DNI remains high. The sharp DNI drops coincide with pour events: because the pyrheliometer is mounted on the concentrator structure, tracking is paused during handling, producing short, artificial dips in the recorded DNI. Once the crucible is recharged, sun-tracking resumes and DNI measurements recover.

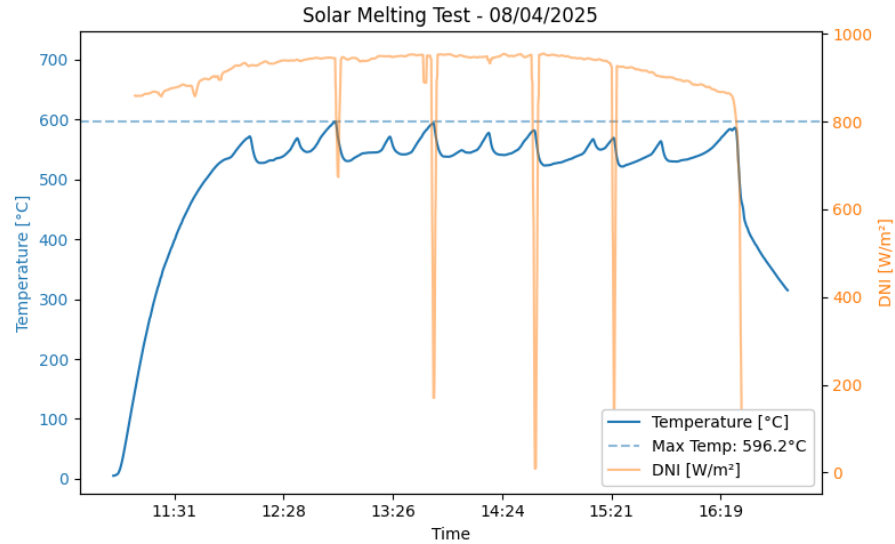


Figure 6. Solar melting test (08 Apr 2025). Crucible temperature (left axis) and measured DNI (right axis).



Figure 7. Solar melting test (08 Apr 2025). Green sand mold with 4 ingots and 1 cylinder of recycled aluminium.

A summary of the performance parameters (melt rate, absorbed heat, useful heat, thermal efficiency and specific energy consumption) is provided in Table 1.

Table 1. Key performance indicators (KPIs) of the Renoval prototype during instrumented outdoor trials (averaged across 21 trials)

Performance Metric	Value (mean)
Melt Rate	195.32 g/h
Absorbed Heat	8,24 kWh
Useful Heat to Melt	0.18 kWh
Thermal Efficiency	2.37 %
Specific Energy Consumption	0.26 kWh/kg

5. Thermodynamic Model & Validation

We developed a low-order lumped-resistance thermal model to reproduce the solar furnace dynamics observed outdoors while remaining fast enough for multi-site annual simulations. The furnace is represented by six virtual nodes with isothermal states and inter-node heat paths as shown in Figure 8:

1. Aluminium Charge
2. Graphite Crucible
3. Firebrick (bottom body)
4. Firebrick (outer body)
5. Firebrick (inner body)
6. Glass-ceramic windows.

Each node has an effective capacity $C = m C_p$ and exchanges heat via solar input and pairwise internal exchange (conduction, cavity radiation and convection), and environmental losses to ambient/sky. Aluminium phase change is handled with an apparent-heat-capacity method across a solidus-liquidus interval. Heat input is the product of measured DNI and an effective optical efficiency. Convection losses are represented with effective heat transfer coefficients for internal cavity and external correlations. Pour/charge events are modelled as discrete mass/enthalpy updated to the Aluminium Charge node. The crucible can temporarily exit the cavity during pouring.

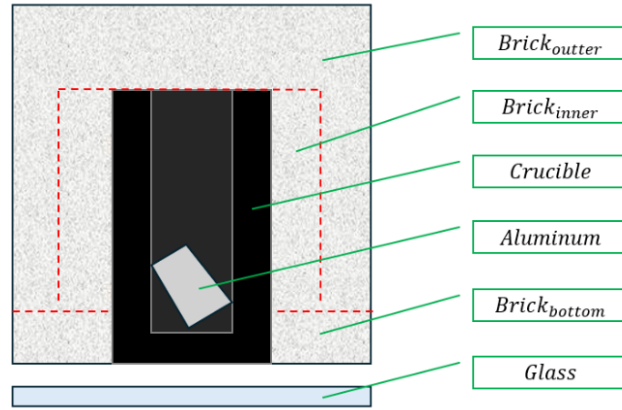


Figure 8. Lumped-node schematic of the Renoval furnace: outer/inner bricks, crucible, aluminium charge, bottom brick, and front window

The properties used in the simulations are the following:

Properties / Material	Aluminum	Graphite Crucible	Insulating Firebrick	Glass-ceramic window
Density (kg m^{-3})	2700	1800	530	2500
Specific Capacity ($\text{J kg}^{-1} \text{K}^{-1}$)	900	1000	1000	1100
Conductivity ($\text{W m}^{-1} \text{K}^{-1}$)	200	100	0.18	2.2
Emissivity (-)	- (not used)	0.99	0.9	0.8

5.1. Governing equations

Solar input is driven by measured DNI and a scalar optical efficiency η_{opt} . For the prototype: reflector aperture A_{ref} is 5.3 m^2 , mirror reflectance ρ is 0.83, effective optical efficiency η_{opt} is 0.45.

The solar input at the aperture is:

$$\dot{Q}_{in}(t) = A_{ref} \rho \eta_{opt} DNI(t) \quad (1)$$

The glass—ceramic absorbs a fix fraction of the radiation ($\alpha = 0.28$) and transmits the rest ($\tau = 0.72$) toward the cavity:

$$\dot{Q}_{glass} = (1 - \tau) \dot{Q}_{in} - \quad (2)$$

$$\dot{Q}_{inc} = \tau \dot{Q}_{in} - \quad (3)$$

The incident power is apportioned primarily to crucible and firebrick (bottom body) according to their proportional area of the cavity.

Dominant intra-cavity pairs (crucible-glass and brick (bottom)-glass) use unit view factors and an effective linearized radiative conductance:

$$h_{rad}(T_i, T_j) = 4 \sigma \epsilon_{eff} \left(\frac{T_i + T_j}{2} + 273.15 \right)^3 \quad (4)$$

$$\epsilon_{eff} = \left(\epsilon_i^{-1} + \epsilon_j^{-1} - 1 \right)^{-1} \quad (5)$$

where i and j are the pairs of bodies mentioned.

The intra-cavity convection h_{cav} has a value of $5 - 10 \text{ W m}^{-2} \text{ K}^{-1}$. Solid-to-solid conduction is represented by constant thermal resistances consistent with the geometry (brick-to-brick paths are less conductive than aluminium-crucible). External losses combine convection and long-wave radiation to ambient/sky as follows:

$$Q_{i, loss} = h_{wind} A_i (T_i - T_{\infty}) + \epsilon_i \sigma A_i (T_i^4 - T_{sky}^4) \quad (6)$$

where i is the body losing energy to the ambient

During pouring, the crucible exits the furnace and losses to the ambient are computed using the equation (6), reproducing the observed cooling pulses during handling.

Aluminium internal energy is advanced in enthalpy space and mapped back to temperature and liquid fraction with a piecewise law: solid below 540°C, linear latent-heat across 540-580°C and liquid above 580°C as shown in equation (7). Aluminium alloy 4032 properties were used.

$$H_{Al}(T) = \int C_{p,Al}(T) dT; \quad C_{p,Al} = \begin{cases} C_{p,solid} & T < T_s \\ C_{p,solid} + \frac{L_f}{T_l - T_s}; & T_s < T < T_l \\ C_{p,liquid} & T > T_l \end{cases} \quad (7)$$

When liquid fraction is equal to 1.0 and $T_{al} \geq 600^\circ \text{C}$, and pour event withdraws 50% of the in-crucible mass and immediately recharges the same mass at 25°C ; the event duration matches the experimental log (around 1 minute).

A synthetic, constant irradiance run ($\text{DNI} = 1000 \text{ W m}^{-2}$) used to illustrate the model's transient behavior is shown in Figure 9. All nodes exhibit a rapid warm-up during the first 60 min: the crucible and brick (inner body, named T_{brick_core}) approach the liquidus band ($540\text{--}580^\circ \text{C}$), while the glass stabilizes at 340°C and the brick (bottom body) and brick (outer body) rise more slowly due to their larger thermal inertia. Two pour events (110 min and 165 min) produce the characteristic, short temperature dips in the crucible and brick (inner body) traces, followed by a quick recovery as tracking resumes. The stair-step in the lower panel confirms that cumulative melted mass increase discretely at each pour (in steps of 0.3 kg). The aluminum curve reflects the enthalpy formulation: its apparent temperature rise is muted around the phase-change interval, even as the melt fraction increases to unity before each pour. Overall, the plot highlights (1) fast start-up under high DNI, (2) the thermal impact of handling events, and (3) the strong coupling between cavity temperatures and melt production.

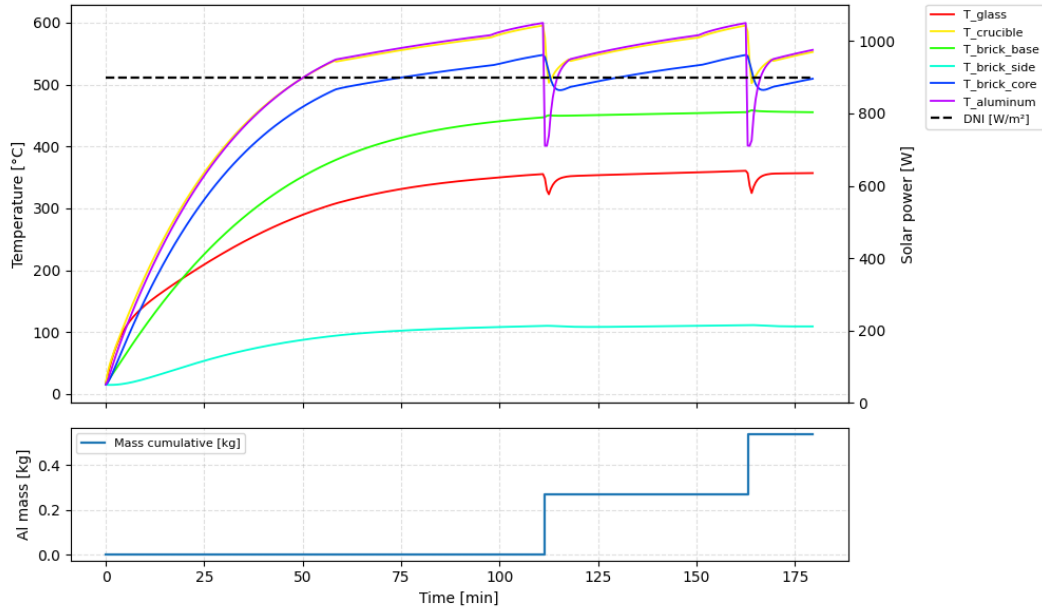


Figure 9. Synthetic constant-DNI run temperatures, pour events, and cumulative melt.

5.2. Model Validation

The comparison between simulated and measured temperature at the crucible-brick interface for a representative validation day (April 7, 2025) together with the measured DNI is shown in Figure 10. Using the measured $DNI(t)$, ambient temperature, and the actual pour/recharge timestamps, the lumped model reproduces the pre-pour thermal ramps and the timing of melt onset with good fidelity. Short deviations occur during manual pour/recharge windows and brief artificial DNI dips appears, due during pour events the structure is paused and temporarily not sun-tracking, so the recorded DNI exhibits these dips. A minimal, physically bounded parameter set was tuned (external heat transfer coefficient, inner cavity heat transfer coefficient, key contact resistances, optical efficiency within simulated optical bounds). The goodness-of-fit metric is the temperature RMSE at the crucible–inner-brick interface; on the day shown the model achieves $RMSE = 31.23^\circ\text{C}$ with accurate onset timing.

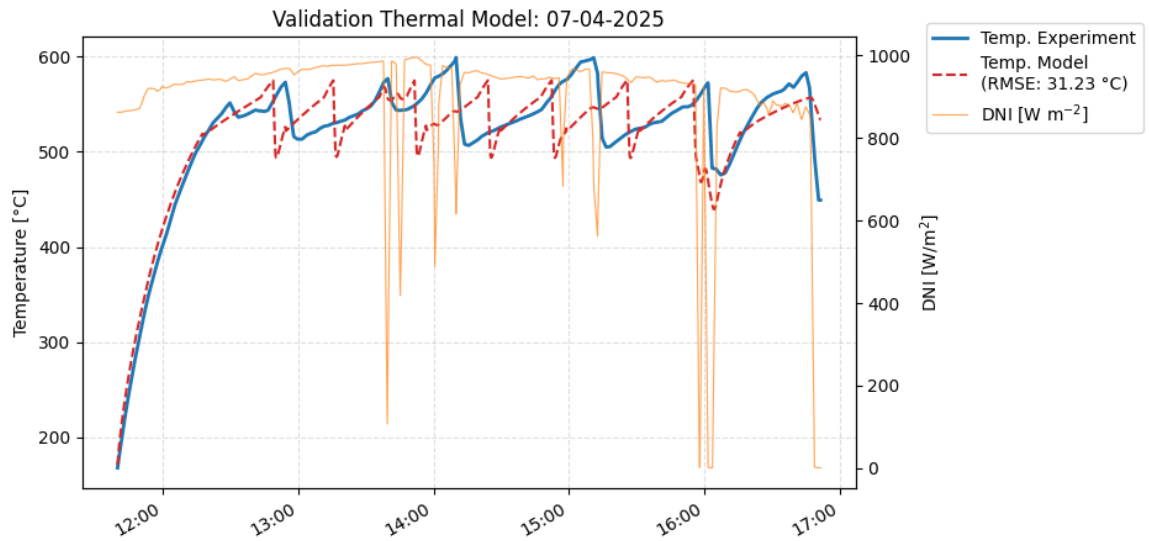


Figure 10. Validation of the lumped thermal model on April 7, 2025: measured and simulated temperature at the crucible–inner-brick interface and measured DNI

5.3. Energy ledgers

To attribute where the solar input goes inside the furnace, we track energy ledgers that balance every joule entering, circulating through, and leaving the lumped network at each time step. Ledgers are signed and time-integrated over a user-selected interval; internal exchanges cancel in the global sum, so the energy balance closes. At each time step, it's being recorded:

1. Solar input ledger: This ledger records the irradiance absorbed or transmitted to each body after optics and window effects.
2. Environmental-loss ledger: Records the net outflows to ambient/sky and for the crucible while pouring outside the cavity.
3. Internal-exchange ledger: Records the heat transfer through conduction in between the bodies, allowing to determine which body is heating each one.
4. Sensible energy: This ledger is equivalent to the body internal energy, calculated with the temperature of each body (for aluminium the ledger considers the latent enthalpy).

Those ledgers allow to analyse the energy balance and an attribution by pathway over a user-selected interval.

A representative diagnosis was developed using the energy ledgers for a 3-hour period at a $DNI = 1000 \text{ W m}^{-2}$ and $T_{amb} = 15^\circ\text{C}$.

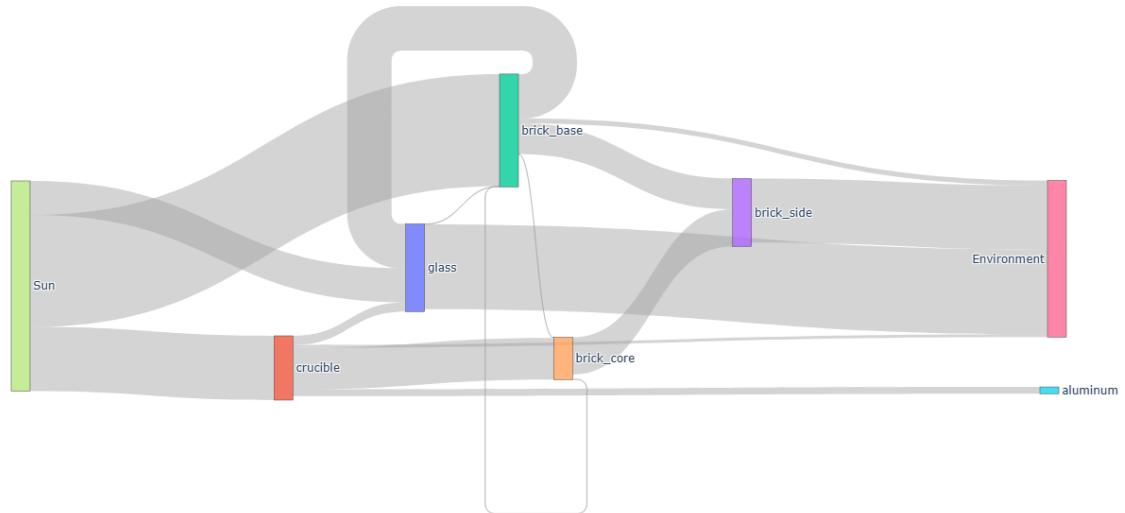


Figure 11. Energy-ledger Sankey for a 3-h synthetic case.

The incident solar energy is 7.07 kWh. External losses dominate at 5.26 kWh (74.4% of input), split primarily between the front glass 2.85 kWh (40.3% of input; 54% of losses) and the side walls 2.15 kWh (30.4% of input; 41% of losses). The remaining 1.81 kWh (25.6%) is stored in the solids, led by the bottom firebrick 1.09 kWh (15.4% of input). Only 0.23 kWh (3.3% of input) reaches aluminium as useful melting energy over this window.

The ranked internal transfers clarify the dominant routes: brick_base → glass (1.49 kWh) and brick_base → brick_side (1.03 kWh) show that heat captured by the base migrates towards well-coupled boundaries; brick_core → brick_side (1.25 kWh) adds to side-wall losses. Leakage from the crucible back into the refractory is evident (crucible → brick_core 1.40

kWh; crucible → glass 0.31 kWh), whereas the productive path crucible → aluminium is only 0.23 kWh.

6. Discussion

6.1.Design and manufacturing

Renoval demonstrates that an annular Fresnel architecture can be fabricated locally with commodity materials and straightforward processes (laser-cut acrylic mirrors, stainless-steel structure, off-the-shelf slewing drives). Segmenting rings to keep individual pieces below ~0.5 m limited self-weight deflection and simplified handling. The switch from an initial 20 cm plate to a graphite crucible receiver traded peak optical efficiency for process functionality (directly heated melt pool with industrial handling and pouring), which is essential for scrap remelting workflows rather than generic flux demonstrations.

Local manufacturing proved strategic: it compressed iteration cycles, built supplier know-how, and enabled fast redesigns (e.g., receiver geometry, window material) without long lead times. This capability is a prerequisite for any transition from experimental rigs to deployable industrial equipment in Chile.

6.2.Operation and handling

Outdoor trials established a repeatable pour/recharge workflow: keep a thin liquid pool, pour ~50 % when the bath reaches liquidus + 10 °C and immediately recharge to recover coupling. Handling intervals necessarily perturb the thermal state; because the pyrheliometer was mounted on the concentrator, pours briefly paused tracking and produced artificial DNI dips in the log—an instrumentation artefact rather than a resource fluctuation. Decoupling the DNI sensor and minimizing out-of-cavity time are straightforward operational improvements.

6.3.Energy-pathway diagnostics

The Pareto of loss mechanisms is clear—window → side walls → refractory inertia (Fig. 10). First-order levers are: (i) reduce the window's long-wave exchange (low- ϵ /IR-reflective glazing) and the view factors from hot refractories (baffles/secondary cavity), (ii) cut side-wall exchange via emissivity control and added insulation, and (iii) lower refractory thermal mass (e.g., microporous or fiberboard base) to shorten warm-up and divert energy to melt. In parallel, strengthen melt coupling by increasing the optical/radiative share onto the crucible (raise view factor of crucible, improve view factor to the melt) and by limiting crucible–brick conduction.

Using a representative melt enthalpy of 0.27 kWh kg⁻¹, every 1 kWh redirected to aluminium yields 3.7 kg of additional melt. For example, a 30% reduction in window losses (baseline 2.85 kWh) saves 0.86 kWh, which could translate to 3.2 kg of extra aluminium melt – subject to the fraction of saved energy that is routed through the productive crucible – aluminium pathway.

6.4.Industrial relevance and local capability

A frequent limitation of high-flux solar facilities is that they remain experimental test beds without industrial handling of scrap, controlled pouring, or validated, metered campaigns. Renoval addresses that gap: it integrates scrap handling and pour operations, shows metered melt under outdoor conditions, and provides a validated low-order model that connects measurements to actionable design changes. Crucially, the prototype was designed and built in Chile, creating a pathway for local suppliers and foundries to adopt low-emission remelting solutions aligned with domestic recycling needs.

7. Conclusions and Outlook

We designed, fabricated, and field-tested Renoval, a compact annular Fresnel concentrator–receiver for aluminium scrap remelting. Twenty-one outdoor trials established a repeatable pour/recharge workflow, with a maximum daily melt of 1.71 kg (April 8, 2025). A six-node lumped-parameter thermal model—calibrated with a minimal, bounded set—reproduced pre-pour ramps and onset timing with RMSE = 31.23 °C, and the energy-ledger analysis revealed a clear Pareto of losses: front window → side walls → refractory inertia, with limited direct coupling to the melt. The combination of local manufacturability and diagnostic modelling provides a credible foundation for scaling from prototype to deployable equipment.

For deployment in Chile’s aluminium-recycling value chain, the next steps are: (a) annual performance simulation across multiple sites and duty cycles (using the validated low-order model), (b) techno-economic assessment (specific energy consumption, LCOH vs. gas/electric baselines), (c) an industrial pilot with continuous or semi-continuous pouring hardware, and (d) supplier development for window coatings, refractory kits, and control hardware manufactured domestically. These steps position Renoval-type systems to contribute to low-emission aluminium remelting in Chile while building local industrial capability.

8. Author contributions

Pablo Castillo: Methodology (equal); Software (lead); Writing—review & editing. Cristopher Rozas: Methodology (equal); Writing—original draft. Francisco Fuentes: Supervision. Ivan Muñoz: Project administration. All authors have read and approved the final manuscript and agree to be accountable for all aspects of the work.

9. Competing interests

The authors declare that they have no competing interests.

10. Funding

This work was supported by CORFO under grant Crea y Valida, ID 23CVI-241439. The funder had no role in study design, data collection and analysis, decision to publish, or preparation of the manuscript.

11. Acknowledgement

Authors acknowledge the generous financial support provided by ANID under project Fraunhofer CSET CTI230004.

12. References

1. International Energy Agency (IEA), *Renewables 2024: Analysis and Forecast to 2030*. Paris, France: IEA, Oct. 2024. [Online]. Available: <https://www.iea.org/reports/renewables-2024>. Accessed: Mar. 11, 2025.
2. International Energy Agency (IEA), “Aluminium: Tracking Clean Energy Progress 2023.” [Online]. Available: <https://www.iea.org/energy-system/industry/aluminium#tracking>. Accessed: Mar. 11, 2025.
3. GlassPoint, “Ma’aden Solar 1.” [Online]. Available: <https://www.glasspoint.com/projects/maaden-solar>. Accessed: Mar. 11, 2025.

4. PROMES-CNRS, "Solar furnaces and concentrating solar systems," facility page, Odeillo, France. [Online]. Available: <https://www.promes.cnrs.fr>. Accessed: Aug. 28, 2025.
5. Plataforma Solar de Almería (PSA), "SF-60 – Solar Furnaces," facility page. [Online]. Available: https://www.psa.es/en/facilities/solar_furnaces/sf60.php. Accessed: Aug. 28, 2025.
6. K. Liang, K. Xue, H. Zhang, H. Chen, and J. Ni, "Design and performance analysis of an annular Fresnel solar concentrator," *Energy*, vol. 210, p. 118594, 2020, doi: 10.1016/j.energy.2020.118594.
7. K. Liang, H. Zhang, H. Chen, D. Gao, and Y. Liu, "Design and test of an annular Fresnel solar concentrator to obtain a high-concentration solar energy flux," *Energy*, vol. 214, p. 118947, 2021, doi: 10.1016/j.energy.2020.118947.
8. Kipp & Zonen B.V., CHP 1 Pyrheliometer – Instruction Manual, ver. 0811. Delft, The Netherlands: Kipp & Zonen B.V., 2008. [Online]. Available: <https://www.kippzonen.com>. Accessed: Sep. 23, 2025.
9. Omega Engineering, "XCIB Series: High-Temperature Inconel Overbraided Ceramic Fibre Insulated Thermocouples." [Online]. Available: <https://www.omega.co.uk/pptst/XCIB.html>. Accessed: Sep. 30, 2025.